INORGANIC CHEMISTRY FRONTIERS

RESEARCH ARTICLE

View Article Online
View Journal | View Issue

Cite this: *Inorg. Chem. Front.*, 2023, **10**, 5462

A UV solar-blind nonlinear optical crystal with confined π-conjugated groups†

Xianyu Song,[a,b] Zhipeng Du,[a,b] Belal Ahmed,[d] Yanqiang Li,[b] Yang Zhou,[b] Yipeng Song,[b] Weiqi Huang,[b] Jieyu Zheng,[b] Junhua Luo [b,c] and Sangen Zhao *[b,c]

Received 1st July 2023,
Accepted 6th August 2023

DOI: 10.1039/d3qi01226c

rsc.li/frontiers-inorganic

UV nonlinear optical (NLO) crystals producing short-wavelength lasers through the second harmonic generation (SHG) process have great significance in the advanced laser field. However, high-performance UV NLO crystals, especially in the UV solar-blind region, are still scarce. In this work, a UV solar-blind NLO compound $Rb[PO_2(NH)_3(CO)_2]\cdot 0.5H_2O$ (RPNCO) is obtained through the ion-exchange reaction. Remarkably, the RPNCO compound exhibits an excellent balance within a wide UV transparency window (absorption edge at 220 nm), a strong SHG response (4.2 × KH_2PO_4), and suitable birefringence (Δn = 0.055@550 nm). Structural analyses and first-principles calculations reveal that the desirable optical properties of RPNCO are attributed to the confined π-conjugation effect of $[PO_2(NH)_3(CO)_2]$ asymmetric groups, in which the non-π-conjugated $PO_2(NH)_2$ tetrahedral group partially decouples the π-conjugated interactions. We believe that this research work can help provide new ideas for the rational design of UV solar-blind NLO crystals.

Introduction

Coherent lasers with nonlinear optical (NLO) crystals generated by direct all-solid-state technology are playing an important role in many fields, as required by technological advances and the development of modern laser devices.[1–5] In particular, UV solar-blind NLO crystals with a transmission range of 200–280 nm are very important in frontier fields such as security of communication networks, precision microfabrication, and optical data storage.[6–11] Thus far, several characteristic properties have been found to be essential for a good solar-blind NLO crystal such as (1) excellent second harmonic generation (SHG) efficiency for laser conversion, (2) a wide bandgap for the transference of SHG and incident lasers, and (3) suitable birefringence to eliminate the dispersion of SHG and incident lasers.[12,13] Moreover, it is tough to satisfy all these criteria in a specific crystal at the same time since they are mutually exclusive. For example, the bandgap is generally inversely related to the SHG efficiency of NLO crystals.[14] The microscopic functional groups intrinsically regulate the optical properties of macroscopic crystalline materials based on the fundamental structure–property relationships. Depending on the traditional functional groups, the design of new optical crystalline materials with better performance than the traditional NLO crystals is still challenging for researchers. Hence, the construction and exploration of NLO crystals consisting of novel microscopic functional groups are necessary for the development of laser technology.

Recently, researchers have reported several strategies to effectively design novel NLO functional groups.[15–20] Chen's group has proposed the confined π-conjugation principle. It involves restriction by non-π-conjugated groups to reduce π-conjugated interactions between the units, thereby increasing the bandgap while maintaining a large optical anisotropy. Based on this principle, introducing the carbonophosphate group enhanced the birefringence value (0.121@532 nm) and the bandgap (6.9 eV) simultaneously in the reported compound $Sr_3Y[PO_4][CO_3]_3$. In the carbonophosphate structure, π-conjugated $[CO_3]^{2-}$ and non-π-conjugated $[PO_4]^{3-}$ are not directly linked.

We assume that when the π-conjugation unit and the non-π-conjugated unit unite directly into a new group through covalent bonds, the confined π-conjugated effect will be increased, thereby increasing the bandgap while maintaining a large optical anisotropy. Guided by this idea, through the

[a]College of Chemistry, Fuzhou University, Fuzhou 350116, China
[b]State Key Laboratory of Structural Chemistry, Fujian Institute of Research on the Structure of Matter, Chinese Academy of Sciences, Fuzhou 350002, China
[c]Fujian Science & Technology Innovation Laboratory for Optoelectronic Information of China, Fuzhou 350108, China
[d]Department of Chemistry, Shahjalal University of Science and Technology, Sylhet 3114, Bangladesh

†Electronic supplementary information (ESI) available: Details of crystal photograph, powder XRD patterns, TG–DTA curves, the bandgap from theoretical calculations, *etc*. CCDC 2277510. For ESI and crystallographic data in CIF or other electronic format see DOI: https://doi.org/10.1039/d3qi01226c

screening of known compounds, we selected and synthesized $Rb[PO_2(NH)_3(CO)_2]\cdot 0.5H_2O$ (RPNCO) with a non-centrosymmetric (NCS) structure.[21–23] It is shown that RPNCO exhibits a large SHG response of about 4.2 × KH_2PO_4 (KDP), a short absorption edge of about 220 nm, and a suitable birefringence of about 0.055@550 nm.

Experimental section

Synthesis

RPNCO single crystals were synthesized by the ion exchange method. First, $Na[PO_2(NH)_3(CO)_2]$ powder was prepared by a simple low-temperature solution method according to previous reports.[21,22] 1.04 g of Rb_2CO_3 (4.5 mmol, Adamas, 99%) and 5.29 g of ion exchange resin were thoroughly mixed in 20 mL of deionized water at room temperature. Then the mixed solution was loaded onto the ion exchange column. The ion exchange resin was then thoroughly rinsed with deionized water to eliminate excess H^+. Following that, 5 mL of $Na[PO_2(NH)_3(CO)_2]$ (0.187 g, 1 mmol) solution was put onto the column by itself. The solution was collected and then evaporated at room temperature. After a few weeks, colorless block-shaped RbPCNO single crystals were successfully grown. The obtained RbPCNO microcrystals were dissolved in deionized water, and single crystals several millimeters in size were obtained by solution volatilization (Fig. S1†).[24]

Results and discussion

The mapping of elemental scanning electron microscope analysis shows that elements Rb, P, O, N, and C are uniformly present on a single crystal of the title compound RPNCO (Fig. 1a). The purity of the RPNCO compound has been confirmed using the powder X-ray diffraction (PXRD) pattern through the good matching with the simulated PXRD pattern (Fig. 1b). The surface of the reported single crystal RPNCO remained nearly unaltered after exposure to air at room temperature for two weeks (Fig. S2†). Single crystals of RPNCO that were left for more than two weeks were milled and subjected to PXRD tests, which showed a good match with the original PXRD pattern of the compound (Fig. S3†), indicating that the compound has good stability in air. The presence of elements Rb, P, C, N, and O in RPNCO was confirmed by energy-dispersive X-ray spectroscopy (EDX) (Fig. S4†).

Single-crystal X-ray diffraction (SCXRD) analysis was performed to illustrate the structure of the title compound RPNCO. RPNCO crystallizes in the NCS monoclinic space group *Cc* (No. 9) consisting of the following crystallographic parameters: a = 6.6882(2) Å, b = 32.5229(10) Å, c = 6.8991(2) Å, β = 94.173(2)°, Z = 4, and V = 1496.71(8) Å^3 (crystallographic details of the title compounds are shown in Tables S1–S5†). The asymmetric unit is composed of two Rb^+ cations, two independent $[PO_2(NH)_3(CO)_2]^-$ moieties, and one crystalline H_2O molecule. A non-π-conjugated $[PO_2(NH_2)]$ tetrahedron

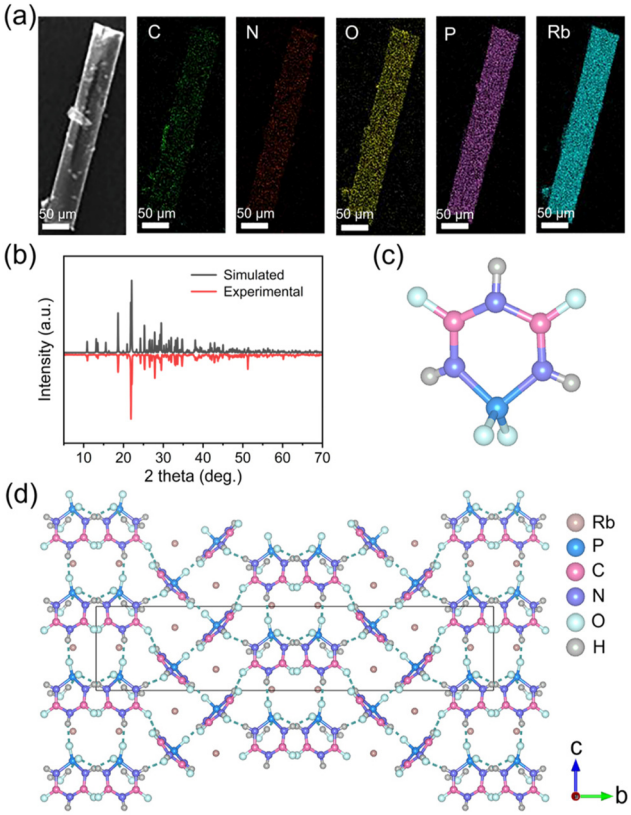

Fig. 1 (a) The mapping of elemental scanning electron microscope analysis. (b) The experimental and calculated PXRD patterns for RPNCO. (c) The $[PO_2(NH)_3(CO)_2]^-$ building block containing a six-membered ring. (d) The representation of the crystal structure of RPNCO along the *a*-axis.

connects to two π-conjugated planar triangle moieties through covalent bonds and forms the six-membered anionic $[PO_2(NH)_3(CO)_2]^-$ ring (Fig. 1c). The hydrogen bonding networks are built through the connection of the $[PO_2(NH)_3(CO)_2]^-$ moiety, resulting in a three-dimensional framework (Fig. 1d). Rb cations and H_2O molecules occupy the holes of the framework to keep the steadiness of the structure. The hydrogen bonding distances are 2.773–2.920 Å (see Table S6†). It is noteworthy that the anionic six-membered $[PO_2(NH)_3(CO)_2]^-$ groups in the structure show four various orientations. Among them, two groups of $[PO_2(NH)_3(CO)_2]^-$ are uniformly aligned in the same direction, whereas the other two groups are situated in different directions. The reported structural arrangement may not be the best orientation to generate a large SHG efficiency based on the anionic group theory.[25]

The differential thermal and thermogravimetric analyses suggested that the thermal stability of RPNCO is maintained up to 422 K (Fig. S5†). The endothermic peak suggests that the compound loses weight above this temperature due to the release of the crystalline H_2O molecules. The weight loss of RPNCO for the first step of the curve is 3.47%, which coincides with the calculated value of crystalline H_2O molecules (3.49%).

The UV-Vis-NIR transmission spectrum for RPNCO was collected at wavelengths 200–800 nm. The absorption edge of RPNCO resides at the wavelength 220 nm of the UV solar blind region, and the corresponding bandgap is 5.64 eV (Fig. 2a). Fig. 2b shows the RPNCO single crystal used for the transmission spectrum test.

The SHG efficiency for the polycrystalline samples of the NCS polar crystal RPNCO was measured at the wavelength 1064 nm using the Kurtz–Perry method.[26] With the increase of particle size, the SHG intensity increases, which indicates a phase-matchable behavior of RPNCO (Fig. 2c). Furthermore, comparison of the SHG intensity shows that RPNCO has a SHG intensity of about 4.2 × KDP in the 74–124 μm particle size range (Fig. 2d). It is noted that the SHG efficiency of the reported RPNCO is relatively higher than that of previously reported compounds containing π-conjugated rings, such as $Y_5(C_3N_3O_3)(OH)_{12}$ (2.5 × KDP) and $Yb_5(C_3N_3O_3)(OH)_{12}$ (3.8 × KDP),[27] $CsAlB_3O_6F$ (2.0 × KDP),[28] $CsZn_2B_3O_7$ (1.5 × KDP),[29] $(C_5H_6ON)^+(H_2PO_4)^-$ (3.0 × KDP),[11] $NaRb_{0.84}Cs_{0.16}HC_3N_3O_3{\cdot}2H_2O$ (3.0 × KDP),[30] $(C_4H_6N_3)^+(H_2PO_3)^-$ (2.0 × KDP),[31] and $K_3C_6N_7O_3{\cdot}2H_2O$ (4.0 × KDP).[32]

The birefringence value of RPNCO was estimated using a polarizing microscope. Fast and slow polarized lights were observed after passing light with a wavelength of 550 nm into an anisotropic single crystal. The retardation R, obtained as $R = d \times (n_s - n_f) = d \times \Delta n$,[33] is produced by fast and slow polarized light while propagating along the crystal, where d, Δn, n_f, and n_s represent the thickness, birefringence, and refractive index for fast and slow polarized light, respectively. The RPNCO crystal exhibits its original interference color as a third-order pink under orthogonally polarized light (Fig. 3a). The color of the crystal turns black in the Berek compensator, which indicates the achievement of extinction (Fig. 3b). The crystal oriented in the $(0\bar{1}0)$ plane was determined by SCXRD

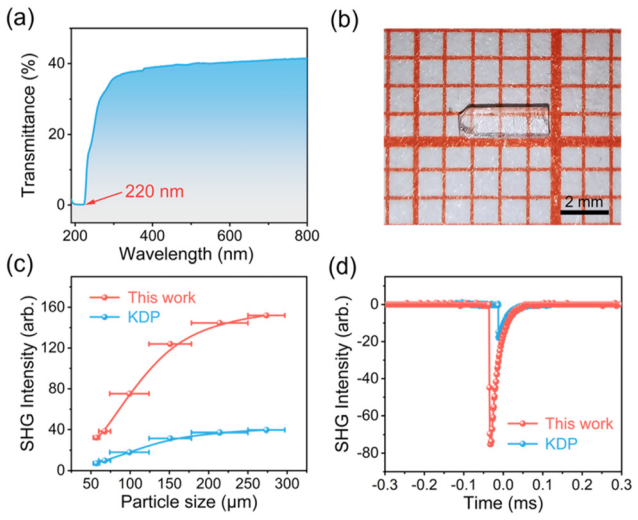

Fig. 2 (a) The transmittance spectrum of the RPNCO crystal. (b) The RPNCO single crystal used for the test of the transmittance spectrum (c) Presentation of SHG efficiency with the size of the particle for RPNCO at a wavelength of 1064 nm. (d) SHG efficiency of RPNCO at 1064 nm.

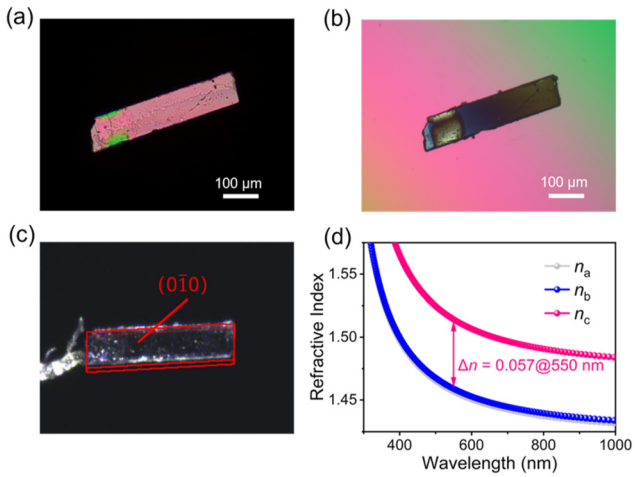

Fig. 3 (a) The original interference color of the RPNCO single crystal observed in orthogonally polarized light. (b) Attainment of extinction for the crystal. (c) The crystal orientation of the selected RPNCO plate determined by SCXRD. (d) The wavelength and calculated refractive indices relationship for RPNCO.

(Fig. 3c). The observed optical path difference is 1662.47 nm at a wavelength of 550 nm and the thickness of the single crystal is 30.50 μm (Fig. S6†). The measured birefringence of RPNCO in the $(0\bar{1}0)$ plane is $\Delta n_{(0-10)exp}$ = 0.055@550 nm. According to first-principles calculations, the static refractive indices of RPNCO at wavelength 550 nm are n_a = 1.459, n_b = 1.459, and n_c = 1.516. Hence, the calculated birefringence (0.057@550 nm) in the *ac*-plane has a good match to the experimental value (0.055@550 nm) (Fig. 3d). It has been mentioned that the measured birefringence of RPNCO is remarkably higher than that of several reported UV NLO crystals,[34,35] like KDP[34] (0.042@532 nm) and LiB_3O_5[35] (0.043@532 nm).

First-principles calculations were used to explain the optical performance and structure correlation of RPNCO.[36,37] Since GGA can better describe the optical properties and HSE06 is more accurate in describing the eigenvalues of electronic states, two different methods were used to calculate the bandgap.[38,39] The bandgap of RPNCO was calculated using GGA, indicating that it has an indirect bandgap of 4.72 eV (Fig. S7†). Due to the discontinuity of the local density approximation exchange–correlation potential, the description of eigenvalues of electronic states in the GGA is not good enough,[40] but the predicted value is in general agreement with the experimental result (5.64 eV). Further calculation using HSE06 shows an indirect bandgap of 6.39 eV (Fig. S8†), which is in good agreement with the experimental result. The constituent elements for RPNCO are represented in the density of states (DOS) and partial DOS diagram (Fig. 4a). The upper part of the valence band near the forbidden band is occupied by O-2p and N-2p orbitals, whereas the O-2p, N-2p, and C-2p states are found at the lower part of the conduction bands. In particular, the apparent overlap between the P-2p, O-2p, N-2p and C-2p orbitals far from the Fermi level represents strong covalent bonding interactions in the $[PO_2(NH)_2]$ and $[CO(NH)_2]$

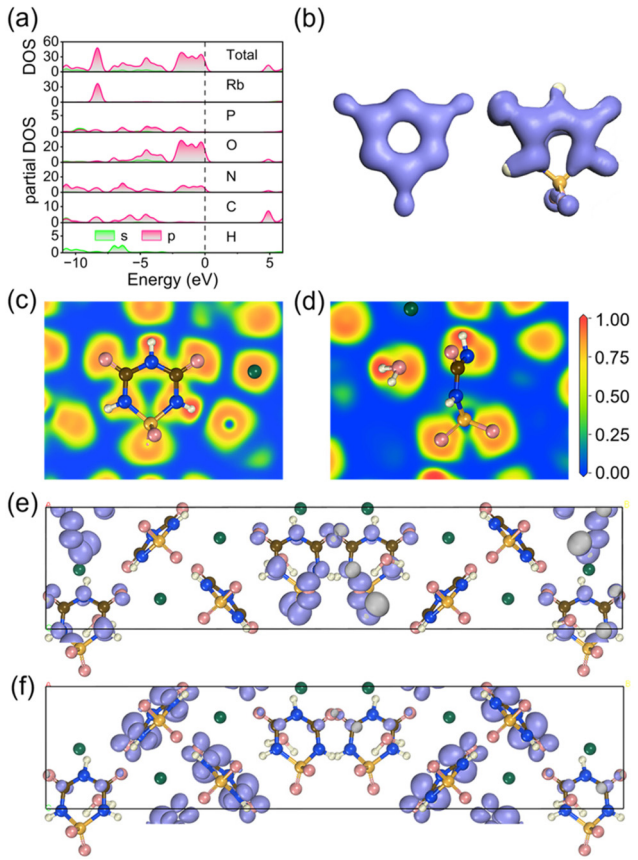

Fig. 4 Theoretical calculations of RPNCO. (a) DOS and partial DOS of RPNCO. (b) The occupied π bonds in $[C_3N_3O_3]^{3-}$ (left) and $[PO_2(NH)_3(CO)_2]^-$ (right). (c and d) Two-dimensional ELF pattern through a six-membered $[PO_2(NH)_3(CO)_2]$ group. Herein, the isovalue increases from blue to red, and the maximum ELF value is scaled to 1. (e) The HOMO map of RPNCO. (f) The LUMO map of RPNCO. The atoms H, C, N, P, O, and Rb are denoted using pale yellow, brown, blue, orange, pink, and green balls, respectively.

units of the $[PO_2(NH)_3(CO)_2]^-$ groups. Thus, the anionic $[PO_2(NH)_3(CO)_2]^-$ groups should be responsible for RPNCO's enlarged bandgap, linear optical properties (*i.e.* birefringence) and second-order NLO properties (*i.e.* SHG), since the transition within electronic states near the Fermi level is sharply related to the optical properties.

The electron localization function (ELF) demonstrates the direct visualization of the contributions of Rb^+, H_2O molecules, and $[PO_2(NH)_3(CO)_2]^-$ anions in RPNCO (Fig. 4c and d). Typical ELF values for covalent bonding are in the range of 0.6–1.0.[41] Strong covalent bonds can be found in the O=P–O bond of the tetrahedral $[PO_2(NH)_2]$ and planar triangle $[CO(NH)_2]$. Moreover, the strong charge density around the $[PO_2(NH)_3(CO)_2]^-$ group exhibits a typical signature of a confined π-conjugated system. The highest occupied molecular orbitals (HOMO) and lowest unoccupied molecular orbitals (LUMO) of RPNCO were calculated to deeply understand the structure–optical properties relationship at the microscopic level (Fig. 4e and f). The HOMO are mostly N-2p and O-2p orbitals (Fig. 4e), and the LUMO contain unoccupied π-orbitals of O-2p, N-2p, and C-2p states (Fig. 4f). Moreover, to compare the conjugation, the occupied π-orbitals for $[C_3N_3O_3]^{3-}$ and $[PO_2(NH)_3(CO)_2]^-$ groups were calculated (Fig. 4b). Highly delocalized π-conjugations are found in the $[C_3N_3O_3]^{3-}$ group. In comparison, the $[PO_2(NH)_3(CO)_2]^-$ group has only σ-bonds on the $[PO_2(NH)_2]$ tetrahedra and no π-electron clouds. It is observed that the π-conjugation system interactions are partly decoupled through the tetrahedral $[PO_2(NH)_2]$ group, and all π-conjugations are confined in $[PO_2(NH)_3(CO)_2]^-$ groups. Therefore, we can conclude that the confined π-conjugation effect gives RPNCO a wider bandgap, which better balances the relationship between SHG, the transparency window, and the birefringence of the crystal.

Conclusions

In summary, we obtained an NLO crystal RPNCO by an ion-exchange method, which reveals significant optical properties such as a broader bandgap of 5.64 eV, a strong SHG response of *ca.* 4.2 × KDP, and suitable birefringence of *ca.* 0.055@550 nm. The SHG performance of the title compound is better than that of most of the reported compounds containing conjugated rings. Its birefringence surpasses that of commercial birefringent crystals with short absorption edges. From calculations based on first principles, we can conclude that the confined π-conjugation effect gives RPNCO a strong SHG response and suitable birefringence while maintaining a wide bandgap, which balances the three properties well. More importantly, guided by the general principle of confined π-conjugation, the $[PO_2(NH)_3(CO)_2]$ groups could provide a new choice for the future design of high-performance NLO crystals in the UV solar-blind region.

Author contributions

X. Song performed the main experimental work and wrote the paper. Z. Du, B. Ahmed, Y. Li, Y Zhou, Y Song, W Huang, and J. Zheng collected some of the experimental data. J. Luo and S. Zhao designed and supervised the overall experiments. All the authors discussed and co-wrote the manuscript.

Conflicts of interest

The authors declare no conflict of interest.

Acknowledgements

The authors acknowledge the financial support for this work from the National Natural Science Foundation of China (22122507, 22193042, 21833010, 61975207, and 21921001), the Natural Science Foundation of Fujian Province (2022J02012), the Youth Innovation Promotion Association of the Chinese

Academy of Sciences (Y202069), and the Key Research Program of Frontier Sciences of the Chinese Academy of Sciences (ZDBS-LY-SLH024), and Fujian Institute of Innovation (FJCXY18010201) in Chinese Academy of Sciences.

References

1 D. Cyranoski, Materials science: China's crystal cache, *Nature*, 2009, **457**, 953–955.
2 D. F. Eaton, Nonlinear optical-materials, *Science*, 1991, **253**, 281–287.
3 Y. Li, C. Yin, X. Yang, X. Kuang, J. Chen, L. He, Q. Ding, S. Zhao, M. Hong and J. Luo, A nonlinear optical switchable sulfate of ultrawide bandgap, *CCS Chem.*, 2021, **3**, 2298–2306.
4 Y. Q. Li, J. H. Luo and S. G. Zhao, Local polarity-induced assembly of second-order nonlinear optical materials, *Acc. Chem. Res.*, 2022, **55**, 3460–3469.
5 N. Savage, Ultraviolet lasers, *Nat. Photonics*, 2007, **1**, 83–85.
6 C. Wu, X. Jiang, Z. Wang, H. Sha, Z. Lin, Z. Huang, X. Long, M. G. Humphrey and C. Zhang, UV solar-blind-region phase-matchable optical nonlinearity and anisotropy in a π-conjugated cation-containing phosphate, *Angew. Chem., Int. Ed.*, 2021, **60**, 14806–14810.
7 X. Zhang, L. Kang, P. Gong, Z. Lin and Y. Wu, Nonlinear optical oxythiophosphate approaching the good balance with wide ultraviolet transparency, strong second harmonic effect, and large birefringence, *Angew. Chem., Int. Ed.*, 2021, **60**, 6386–6390.
8 H. Yan, Y. Matsushita, K. Yamaura and Y. Tsujimoto, $La_3Ga_3Ge_2S_3O_{10}$: An ultraviolet nonlinear optical oxysulfide designed by anion-directed band gap engineering, *Angew. Chem., Int. Ed.*, 2021, **60**, 26561–26565.
9 T. Gu, N. Petrone, J. F. McMillan, A. van der Zande, M. Yu, G. Q. Lo, D. L. Kwong, J. Hone and C. W. Wong, Regenerative oscillation and four-wave mixing in graphene optoelectronics, *Nat. Photonics*, 2012, **6**, 554–559.
10 B. Shen, P. Wang, R. Polson and R. Menon, An integrated-nanophotonics polarization beamsplitter with 2.4 × 2.4 μm^2 footprint, *Nat. Photonics*, 2015, **9**, 378–382.
11 J. Lu, X. Liu, M. Zhao, X. B. Deng, K. X. Shi, Q. R. Wu, L. Chen and L. M. Wu, Discovery of NLO semiorganic $(C_5H_6ON)^+(H_2PO_4)^-$: Dipole moment modulation and superior synergy in solar-blind UV regions, *J. Am. Chem. Soc.*, 2021, **143**, 3647–3654.
12 P. S. Halasyamani and J. M. Rondinelli, The must-have and nice-to-have experimental and computational requirements for functional frequency doubling deep-UV crystals, *Nat. Commun.*, 2018, **9**, 2972.
13 C. T. Chen, N. Ye, J. Lin, J. Jiang, W. R. Zeng and B. C. Wu, Computer-assisted search for nonlinear optical crystals, *Adv. Mater.*, 1999, **11**, 1071–1078.
14 J. J. Zhou, H. P. Wu, H. W. Yu, S. T. Jiang, Z. G. Hu, J. Y. Wang, Y. C. Wu and P. S. Halasyamani, $BaF_2TeF_2(OH)_2$: A UV nonlinear optical fluorotellurite material designed by band-gap engineering, *J. Am. Chem. Soc.*, 2020, **142**, 4616–4620.
15 L. Xiong, L. M. Wu and L. Chen, A general principle for DUV NLO materials: π-Conjugated confinement enlarges band gap, *Angew. Chem., Int. Ed.*, 2021, **60**, 25063–25067.
16 M. J. Li, X. Zhang, Z. Y. Xiong, Y. Q. Li, Y. Zhou, X. Chen, Y. P. Song, M. C. Hong, J. H. Luo and S. G. Zhao, A hybrid antiperovskite with strong linear and second-order nonlinear optical responses, *Angew. Chem., Int. Ed.*, 2022, **61**, e202211151.
17 Y. Q. Li, W. Q. Huang, Y. Zhou, X. Y. Song, J. Y. Zheng, H. Wang, Y. P. Song, M. J. Li, J. H. Luo and S. G. Zhao, A high-performance nonlinear optical crystal with a building block containing expanded π-delocalization, *Angew. Chem., Int. Ed.*, 2022, e202215145.
18 H. T. Tian, N. Ye and M. Luo, Sulfamide: A promising deep-ultraviolet nonlinear optical crystal assembled from polar covalent $[SO_2(NH_2)_2]$ tetrahedra, *Angew. Chem., Int. Ed.*, 2022, **61**, e202200395.
19 Y. Q. Li, J. H. Luo, X. H. Ji and S. G. Zhao, A short-wave UV nonlinear optical sulfate of high thermal stability, *Chin. J. Struct. Chem.*, 2020, **39**, 485–492.
20 Y. Zhou, Y. Q. Li, Q. R. Ding, Y. C. Liu, Y. X. Chen, X. T. Liu, X. Y. Huang, L. N. Li, S. G. Zhao and J. H. Luo, Noncentrosymmetric $K_2Mn_3(SO_4)_3F_2{\cdot}4H_2O$ and $Rb_2Mn_3(SO_4)_3F_2{\cdot}2H_2O$ with pseudo-KTP structures, *Chin. Chem. Lett.*, 2021, **32**, 263–265.
21 E. Wirnhier and W. Schnick, A systematic approach to alkali biuretooxophosphates, *Eur. J. Inorg. Chem.*, 2012, **11**, 1840–1847.
22 E. Wirnhier and W. Schnick, $Ca[PO_2(NH)_3(CO)_2]_2$ – The first biuretooxophosphate with a divalent cation, *Z. Anorg. Allg. Chem.*, 2012, **638**, 920–924.
23 Y. Zhou, X. Zhang, M. C. Hong, J. H. Luo and S. G. Zhao, Achieving effective balance between bandgap and birefringence by confining π-conjugation in an optically anisotropic crystal, *Sci. Bull.*, 2022, **67**, 2276–2279.
24 F. Liu, K. Chen and D. Xue, How to fast grow large-size crystals?, *Innovation*, 2023, **4**, 100458.
25 C. T. Chen, Y. C. Wu and R. K. Li, The anionic group-theory of the non-linear optical effect and its applications in the development of new high-quality NLO crystals in the borate series, *Int. Rev. Phys. Chem.*, 1989, **8**, 65–91.
26 S. K. Kurtz and T. T. Perry, A powder technique for evaluation of nonlinear optical materials, *J. Appl. Phys.*, 1968, **39**, 3798.
27 X. H. Meng, X. Y. Zhang, Q. X. Liu, Z. Y. Zhou, X. X. Jiang, Y. G. Wang, Z. S. Lin and M. J. Xia, Perfectly encoding π-conjugated anions in the $RE_5(C_3N_3O_3)(OH)_{12}$ (RE = Y, Yb, Lu) family with strong second harmonic generation response and balanced birefringence, *Angew. Chem., Int. Ed.*, 2023, **62**, e202214848.
28 H. K. Liu, Y. Wang, B. B. Zhang, Z. H. Yang and S. L. Pan, $CsAlB_3O_6F$: A beryllium-free deep-ultraviolet nonlinear optical material with enhanced thermal stability, *Chem. Sci.*, 2020, **11**, 694–698.

29 S. G. Zhao, J. Zhang, S. Q. Zhang, Z. H. Sun, Z. S. Lin, Y. C. Wu, M. C. Hong and J. H. Luo, A new uv nonlinear optical material $CsZn_2B_3O_7$: ZnO_4 tetrahedra double the efficiency of second-harmonic generation, *Inorg. Chem.*, 2014, **53**, 2521–2527.

30 J. Lu, Y. K. Lian, L. Xiong, Q. R. Wu, M. Zhao, K. X. Shi, L. Chen and L. M. Wu, How to maximize birefringence and nonlinearity of π-conjugated cyanurates, *J. Am. Chem. Soc.*, 2019, **141**, 16151–16159.

31 Z. P. Zhang, X. Liu, X. M. Liu, Z. W. Lu, X. Sui, B. Y. Zhen, Z. S. Lin, L. Chen and L. M. Wu, Driving nonlinear optical activity with dipolar 2-aminopyrimidinium cations in $(C_4H_6N_3)^+(H_2PO_3)^-$, *Chem. Mater.*, 2022, **34**, 1976–1984.

32 X. Y. Zhang, X. G. Du, J. H. Wang, F. Y. Wang, F. Liang, Z. G. Hu, Z. S. Lin and Y. C. Wu, $K_3C_6N_7O_3{\cdot}2H_2O$: A multifunctional nonlinear optical cyamelurate crystal with colossal π-conjugated orbitals, *ACS Appl. Mater. Interfaces*, 2022, **14**, 53074–53080.

33 B. E. Sorensen, A revised Michel-Levy interference colour chart based on first-principles calculations, *Eur. J. Mineral.*, 2013, **25**, 5–10.

34 D. A. V. Kliner, F. Di Teodoro, J. P. Koplow, S. W. Moore and A. V. Smith, Efficient second, third, fourth, and fifth harmonic generation of a Yb-doped fiber amplifier, *Opt. Commun.*, 2002, **210**, 393–398.

35 C. T. Chen, Y. C. Wu, A. D. Jiang, B. C. Wu, G. M. You, R. K. Li and S. J. Lin, New nonlinear-optical crystal – LiB_3O_5, *J. Opt. Soc. Am. B*, 1989, **6**, 616–621.

36 M. C. Payne, M. P. Teter, D. C. Allan, T. A. Arias and J. D. Joannopoulos, Iterative minimization techniques for *ab initio* total-energy calculations – molecular-dynamics and conjugate gradients, *Rev. Mod. Phys.*, 1992, **64**, 1045–1097.

37 S. J. Clark, M. D. Segall, C. J. Pickard, P. J. Hasnip, M. J. Probert, K. Refson and M. C. Payne, First principles methods using CASTEP, *Z. Kristallogr.*, 2005, **220**, 567–570.

38 J. P. Perdew, K. Burke and M. Ernzerhof, Generalized gradient approximation made simple, *Phys. Rev. Lett.*, 1996, **77**, 3865–3868.

39 J. Heyd, G. E. Scuseria and M. Ernzerhof, Hybrid functionals based on a screened Coulomb potential (vol. 118, pg 8207, 2003), *J. Chem. Phys.*, 2006, **124**, 219906.

40 R. W. Godby, M. Schluter and L. J. Sham, Trends in self-energy operators and their corresponding exchange-correlation potentials, *Phys. Rev. B: Condens. Matter Mater. Phys.*, 1987, **36**, 6497–6500.

41 A. Savin, R. Nesper, S. Wengert and T. F. Fassler, ELF: The electron localization function, *Angew. Chem., Int. Ed. Engl.*, 1997, **36**, 1809–1832.